# The Biased Filter for Secondary Specie Emissions from the Beam Target of Electric Thrusters


## Abstract

This research aims to enhance the accuracy of data collection during ground testing of ionic thrusters. Specifically, it explores the utilization of a dual-layer biased filter to mitigate emissions from secondary species emission (SSE). SSE, whether charged or neutral, emerges when the ionic particle beam interacts with metal surfaces within the vacuum chamber and peripheral experimental equipment. These emissions lead to contamination and disruptive interference with the accurate processing of experimental data, such as particle density and current measurements. The proposed design introduces a dual-layer charged grid with a defined electric potential. This grid confines the movement of SSE, preventing the rebound of secondary particles, while allowing the incident beam with higher energy and electric potential to traverse through with minimal disruption.


## Introduction

This study begins by qualitatively validating the feasibility of the proposed approach. COMSOL Multiphysics is employed to simulate the particle-field interactions. The simulation encompasses the vacuum chamber, beam target plate, and other setup components, which can be tailored to various real-world scenarios. To ensure versatility, the COMSOL model is parameterized according to the geometric attributes of the testing environment and key particle physics parameters.

The analysis yields direct insights into electric potential, electric fields, and particle trajectories within specific time intervals. For convenience, a MATLAB program is developed to process the data exported from the model, allowing for analysis of the maximum potential along critical geometric axes. Lastly, the findings are summarized in the form of tables and phase diagrams, highlighting key parameters and their respective contributions to overall performance.

In the process, multiple different grid geometries are explored, coupled with different incident potentials and particle counts, to identify the most optimal grid configuration. The optimization process aims to minimize material usage, manufacturing costs, structural complexity, minimal disruption to the testing environment, while maximizing the potential field. In the end, the proposed design is translated into a Solidworks model.

## Theoretical Explanation

Electric thrusters are commonly sealed in metal vacuum chambers equipped with measurement instruments, aiming to replicate the space environment by minimizing the influence of atmospheric conditions. However, a crucial distinction arises: there is no vacuum chamber and the accompanying sensors in space. It is well-established that the incident plasma beam interacts

with these apparatuses, emitting secondary particles, a phenomenon termed the "facility effect" [2]. The subsequent interactions between the incident beam and these secondary species likely underlie the phenomenon of electric thrusters exhibiting luminosity in a vacuum [1].

Given that these secondary species obscure an accurate assessment of electric thruster performance, this study introduces the concept of employing the electric potential field generated by charged wires to impede particles carrying a charge below a certain energy threshold. To substantiate the effectiveness of this design, several conditions are meticulously examined. Firstly, given that the potential of the incident beam significantly surpasses that of the secondary species, the introduced potential should have a minimal impact on the incident beam while effectively obstructing secondary species from recoiling off the beam target and commingling with initial particles. Secondly, the wires can be organized into a dual-layer grid configuration to ensure comprehensive hindrance for both positively and negatively charged secondary species (unfortunately this won't work for neutral species which are rare [?]). Thirdly, a magnetic approach is excluded from consideration due to concerns regarding its applicability to particles with high mass-to-charge ratios.

## Simulation Setup

For the best compatibility and clarity, the simulation process is completed with COMSOL Multiphysics, where the electrostatics (es) and charged particle tracing (cpt) physics are used.

The vacuum chamber is configured as a cylinder with a height of 100 in and a radius of 50 in, featuring circular end surfaces oriented in the z-direction. The wires are uniform cylinders confined to the x or y axes. These wires have a radius of 1/400 inches and adjustable lengths. The geometric attributes of the wires are dictated by a set of pivotal parameters: wires per layer (w_pl), number of layers (w_ly), parallel separation, and vertical clearance (w_vc)[1]. Within each layer, all wires share the same z-coordinate and orientation, maintaining uniform separation at equidistant intervals (parallel separation). The design configurations often comprise even number of layers to ensure bias for charges with either sign. Each layer is either parallel or orthogonal in relation to its adjacent layers[2].

Typically, the assembly can be divided into two parts (referred to as an array in COMSOL), positioned at equidistant but opposing distances from the special center of the cylinder (origin). The distance between the two parts is defined by the parameter "vertical clearance." Meanwhile, the parameter "number of layers" determines the total count of layers present. For clarity, a more explicit notation is introduced as w_ly(a, b), where a signifies the number of layers in the +z-axis direction and b represents the -z-axis direction. In all instances covered by this research, w_ly assumes an even value, a equals b, and w_pl remains uniform across all layers. (If you feel confused, stop reading this section and jump to the results, it's really hard to understand through pure text.)

Particularly noteworthy are scenarios involving 4(2,2) layers, wherein the separation between the two layers is established by a consistent value of 0.05 inches. This is because to the potential of

the two layers could be differing in sign and thus cannot be intersected. All wires bear a charge equivalent to ±w_phi (initially 1000V).

For the particle tracing module, the secondary species are launched hemispherically from the center of the beam target, which is a thin rectangular plate in the xy-plane, centered at z-axis, with a fixed distance of 4in to the layer with least z-coordinate. The z-coordinate of this is automatically adjusted in the model given vertical clearance (w_vc). The launched particles have a predefined mass and fixed kinetic energy, and the resulting speed variation and study length is automatically controlled for convenience in the model. The number of particles per release could also be adjusted. Note that the text in this paragraph describes the final particle tracing setup, step-by-step variations are scrutinized in Stage Delta.

In all cases, the material of the cylinder domain is defined as vacuum, and all wires are made of tungsten (material actually has little impact on performance). The vacuum chamber is also grounded.

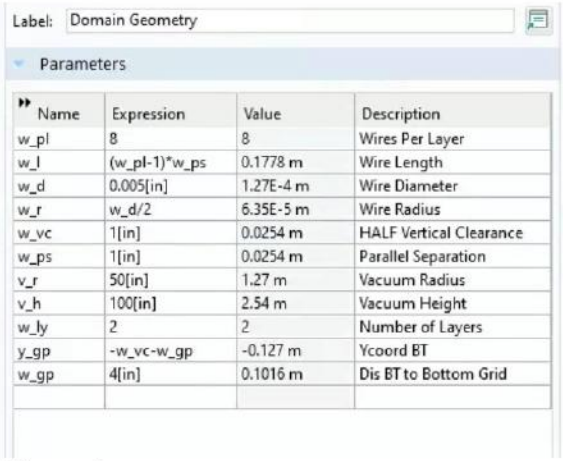

Label: Domain Geometry

Parameters

| Name | Expression | Value | Description |
|---|---|---|---|
| w_pl | 8 | 8 | Wires Per Layer |
| w_l | (w_pl-1)*w_ps | 0.1778 m | Wire Length |
| w_d | 0.005[in] | 1.27E-4 m | Wire Diameter |
| w_r | w_d/2 | 6.35E-5 m | Wire Radius |
| w_vc | 1[in] | 0.0254 m | HALF Vertical Clearance |
| w_ps | 1[in] | 0.0254 m | Parallel Separation |
| v_r | 50[in] | 1.27 m | Vacuum Radius |
| v_h | 100[in] | 2.54 m | Vacuum Height |
| w_ly | 2 | 2 | Number of Layers |
| y_gp | -w_vc-w_gp | -0.127 m | Ycoord BT |
| w_gp | 4[in] | 0.1016 m | Dis BT to Bottom Grid |

Figure 1

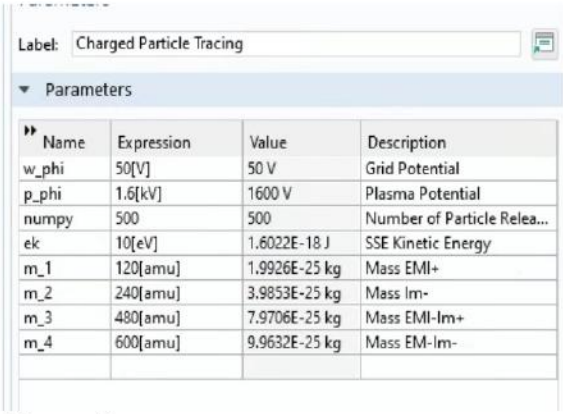

Label: Charged Particle Tracing

Parameters

| Name | Expression | Value | Description |
|---|---|---|---|
| w_phi | 50[V] | 50 V | Grid Potential |
| p_phi | 1.6[kV] | 1600 V | Plasma Potential |
| numpy | 500 | 500 | Number of Particle Relea... |
| ek | 10[eV] | 1.6022E-18 J | SSE Kinetic Energy |
| m_1 | 120[amu] | 1.9926E-25 kg | Mass EMI+ |
| m_2 | 240[amu] | 3.9853E-25 kg | Mass Im- |
| m_3 | 480[amu] | 7.9706E-25 kg | Mass EMI-Im+ |
| m_4 | 600[amu] | 9.9632E-25 kg | Mass EM-Im- |

Figure 2

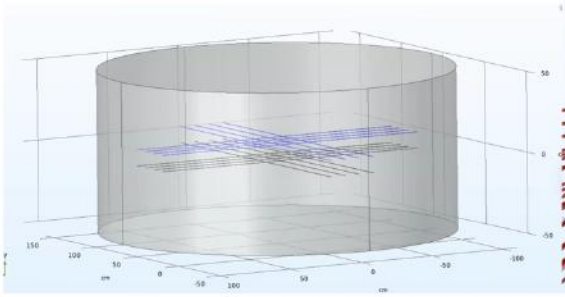

Figure 3

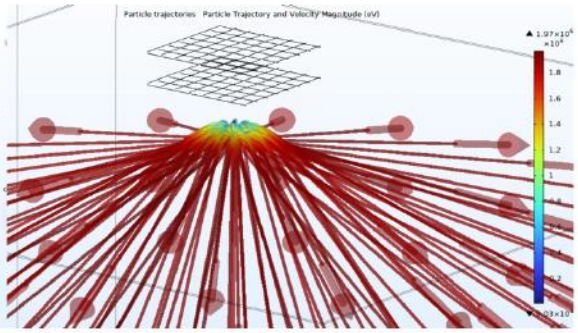

Figure 4

Eg, for the model in Figure 3: Numbers per Layer = 4(2,2), Wires per Layer = 4, Total Wires = 16. The upper part consists of 2 layers with same potential is highlighted with blue, and the lower black part is identical to the upper part, with opposite potential.

Eg, for the model in Figure 4: Numbers per Layer = 4(2,2), Wires per Layer = 8, Total Wires = 32. Potential setting is like that of Figure 3. It basically just cuts the wires' peripheral tails off and makes the grid denser (smaller parallel separation).

## Results

### Stage Alpha (Feasibility Verification using Simple Case)

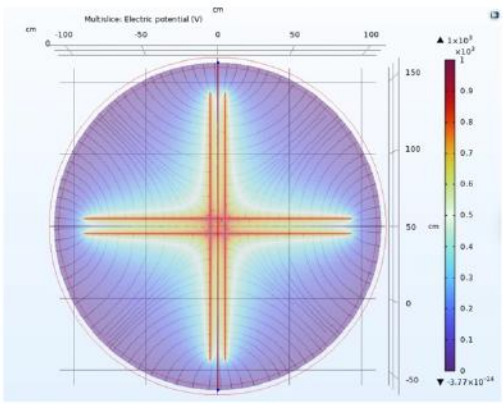

Figure 5

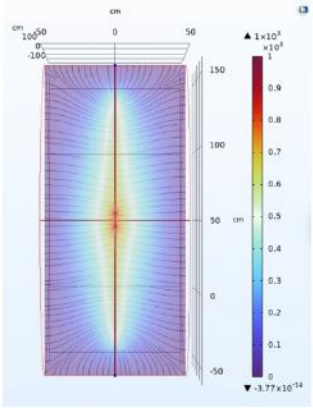

Figure 6

In this stage, four wires within the same xy-plane are assembled in a cross pattern, with the center square having a parallel separation (side length) of 10cm. The grid is sealed in a large cylinder of vacuum with radius of 100cm (~20x in length), and a voltage of +1000V is applied to the grid. Figure 5,6 shows a symmetric electric potential field with physical plausibility. The potential experiences only marginal diminishment in the immediate vicinity of the wires, while its rate of decrease accelerates as it moves farther away. Notably, within the central region responsible for impeding secondary species emissions (SSEs), the field intensifies to roughly 80% of the applied voltage. Figure 7 demonstrates the exact potentials measured along the z (blue) and either x or y axis (green). It is also clear that the outskirts have a rather little contribution to the field, and the geometric center of the grid is a local minimum in the xy-plane.

Given the rather strong field in the central square, this electrostatic biased filter has the potential to successfully block the particles SSEs. Furthermore, three avenues for design enhancement warrant exploration: first, reducing the parallel separation has the potential to elevate the local minima at the geometric center; second, consideration could be given to eliminating the outer sections of the wires, thereby retaining solely the central square; third, an investigation into the impact of vertical clearance remains imperative.

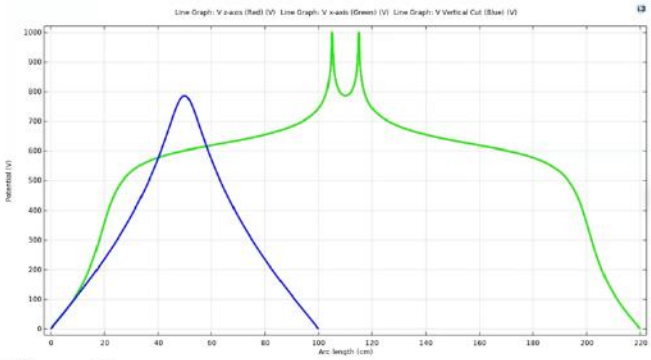

Figure 7

**Stage Beta (Investigations on the effect of Vertical Clearance and Parallel Separation)**

In this stage, we used the similar grid setting as Stage Alpha, and has doubled the layer as well as adjusted the parallel separation (i.e., side length of the square) from 0cm to 20cm. The corresponding change of maximum potential along the central z-axis is measured and plotted in Figure 8. It's clear that the as the parallel separation increases, the electric potential decreases (quite intuitive!). While this model only considers wires with same sign of potential, it's reasonable to infer that the potential follows the same rule if there are two layers of wires with opposite signs of potential.

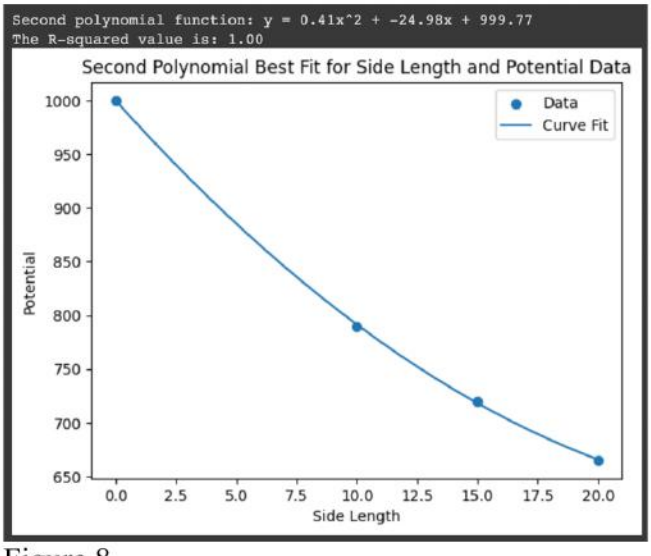


Figure 8

For vertical clearance, a new grid geometry is adopted as shown in Figure 9. The upper four wires are charged with a potential of -1kV and lower four wires are charged with +1kV.

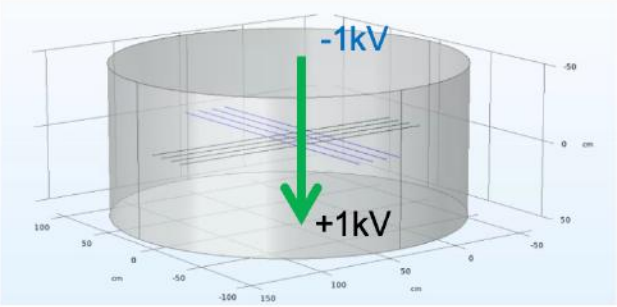


Figure 9

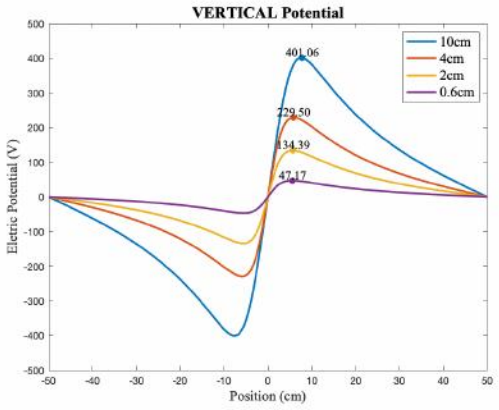


Figure 10

The vertical distance between the two layers of wires was adjusted, ranging from 0.6 cm to 10 cm, and subsequently, the variation in voltage along the central z-axis was plotted using MATLAB (Figure 10). It becomes apparent that there is an increase in electric potential as the vertical separation expands. This phenomenon, initially seeming counterintuitive, finds its rationale in the application of voltages with opposing signs. In such circumstances, closer proximity tends to lead to a more pronounced nullification of potential. Conversely, in cases involving similar potential charges, a reduced vertical clearance would be more helpful. However, it should be noted that within the specific context of our application scenario, the presence of wires carrying opposite charges remains essential.

In conclusion, growth in parallel separation negatively affects the electric potential, while growth in vertical clearance positively affects the electric potential in the scope of this research.

**Stage Gamma (Investigations on the Efficiency of Several Common Geometries)**

In this stage, several easy-to-build and common geometries are investigated. All wires in the following five geometries have equal length and radius. The wires colored in blue and black symbolize a charged potential characterized by uniform magnitude yet opposite sign.

First, Figure 11 represents a very similar geometry in Stage Alpha, but there are four layers of wire placed perpendicular to their neighbors. Especially, the four layers are charged with alternating signs of potential (+-+-, from +z to -z axis). In this case, the maximum potential along the z-axis is measured to be only ±72V out of the supplied 1000V, making it the least efficient design so far. The cause for this phenomenon is discussed in Stage Beta.

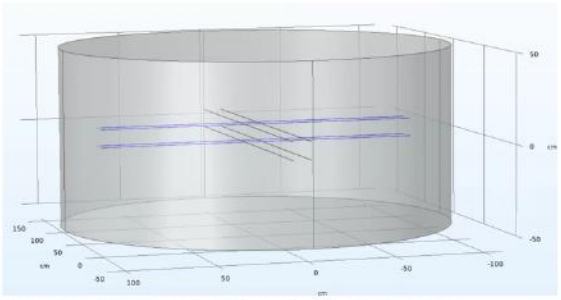
Figure 11 Alternating Perpendicular

Second, Figure 12 is based on identical geometries as in Figure 11. The only difference is that the order in which voltage is supplied has changed from alternating (+_+_) to separating (++__). The maximum potential obtained along the z-axis is ±515V. While this result seems disappointing from the initial 1000V, it demonstrates that the "separating" method to supply voltage is far more efficient than the "alternating" approach.

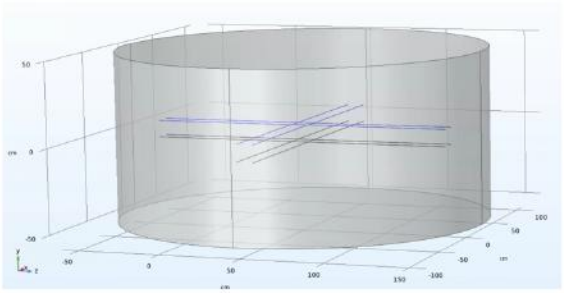
Figure 12 Separating Perpendicular

Third, Figure 13 features an identical geometry as in Figure 9 where the influence of vertical clearance on maximum potential was discussed. The maximum potential obtained is about ±400V. Comparing with the "crossing" geometry in Figure 12, this "straight wires" design offers more manufacturing compatibility with a small sacrifice on max potential.

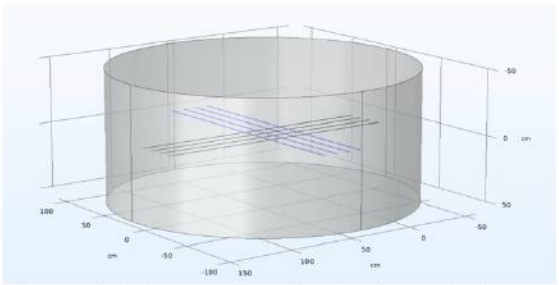
Figure 13 Separating Single (Identical to Figure 9)

Fourth, Figure 14 features twice the number of wires and integrates the geometric advantages of Figure 12 and Figure 13. Consequently, this setup affords a maximum potential of roughly ±580 V, notably surpassing the values obtained from the prior two designs. Moreover, the incorporation of an increased number of wires serves an additional purpose: it contributes to the gradual attenuation of the potential field, resulting in the persistence of a comparatively robust field over a broader spatial expanse.

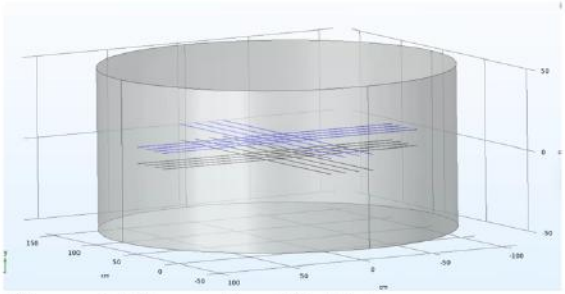

Figure 14 Separating Multiple

Lastly, Figure 15 is based on an identical geometry as Figure 14, but the way voltage is supplied has been changed from “Separating” to “Alternating.” Certainly, this outcome manifests as a substantial reduction in the maximum potential to an astonishing ±26 V, thereby extinguishing any remaining prospects associated with the “alternating” geometry.

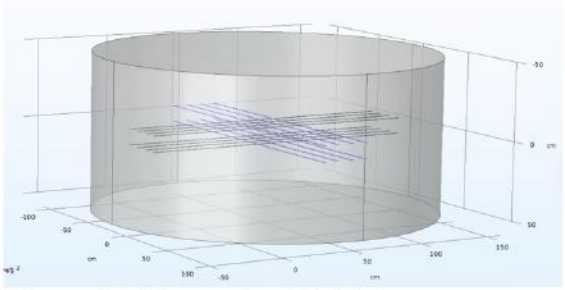

Figure 15 Alternating Multiple

For ease of reference, the models featuring intricate geometric configurations have been succinctly summarized in Table 1. These simulations collectively convey that the most optimal design corresponds to Model No. 5, denoted as the "Separating Multiple" model, wherein the electric potential is applied as depicted in Figure 14. This approach yields a maximum potential amounting to approximately 58% of the provided voltage. It is reasonable to anticipate the perpetuation of this efficiency when extrapolating to scaled variations in both the dimensions and voltage of this geometry.

| Set | Layers/ Set of Layers | Wires/ Layer | Total Wires | Vertical Separation/ Within Set | Side Length | Potential Geometry | Vertical Potential Max | Ref Page |
|---|---|---|---|---|---|---|---|---|
| 1 | 4 (2, 2) | 2 | 8 | 10 / 0 cm | 10 cm | Mono | + 900 V | Stg Alpha |
| 2 | 2 (1, 1) | 4 | 8 | 10 cm | 10 cm | Separate | ± 400 V | Figure 13 |
| 3 | 4 (2, 2) | 2 | 8 | 10 / 0.5 cm | 10 cm | Separate | ± 515 V | Figure 12 |
| 4 | 4 (2, 2) | 2 | 8 | 10 / 0.5 cm | 10 cm | Alternating | ± 72 V | Figure 11 |
| 5 | 4 (2, 2) | 4 | 16 | 10 / 0.5 cm | 10 cm | Separate | ± 580 V | Figure 14 |
| 6 | 4 (2, 2) | 4 | 16 | 10 / 0.5 cm | 10 cm | Alternating | ± 26 V | Figure 15 |
| 7 | 4 (2, 2) | 8 | 32 | 2 in | 1 in | Separate | 50 | P45 + |

Table 1

**Stage Delta (Particle Tracing)**

Subsequent to the identification of the optimal geometry in the preceding phase, the COMSOL simulation is enhanced with the incorporation of the charged particle tracing (cpt) physics interface. This integration is based on the geometry depicted in Figure 13 (denoted as Set 2 in Table 1, not Figure 14 for simulation simplicity). The purpose of this integration is to establish a vital link between the potential field and the trajectories of secondary emission particles—a fundamental step to corroborate the feasibility of the potential simulations. Notably, the primary objective underlying the design of these grids revolves around their capacity to effectively inhibit the passage of all secondary emissions.

The implementation unfolds through a structured sequence of steps:

First, a set of 20 negatively charged particles (electrons), each carrying distinct kinetic energies, is launched from the uppermost point along the z-axis. These particles exhibit a -z velocity, thereby validating the design's efficacy in halting the progression of particles.
Second, the particle count is augmented to enhance the clarity of trajectory visualization and spatial distribution.

Third, electrons are substituted with positrons, maintaining all other parameters unchanged. This alteration serves to ascertain the grid's capability to obstruct particles bearing either positive or negative charges. This test is imperative due to the employed separating geometry. In such a configuration, the repulsion of electrons (caused by the initial negative layers) could potentially lead to the attraction and acceleration of positively charged species, thereby increasing the challenge of traversing the grid—a concept akin to the rationale behind favoring a larger vertical clearance over a smaller one.

In the end, a phase diagram is established to visualize the impact of the two most important parameters: “parallel separation” and “vertical clearance.”
Fourth, a grounded metal plate is introduced into the simulation to replicate the presence of a beam target and associated instruments, reminiscent of their real-world counterparts within vacuum chambers.

Lastly, the grid is truncated, and the launch mechanism transitions from a uniform beam to a hemispherical launch originating from the beam target surface. This modification aims to emulate real-world scenarios more faithfully. Additionally, the simulation introduces heavier charged species. Furthermore, the capacity of the geometry to allow the passage of an incident beam bearing 1600 volts is tested, assessing potential interference levels. This evaluation aims to establish that the geometry exclusively impedes low-energy secondary species emissions.

Ultimately, a phase diagram is established, offering a graphical representation of the influence exerted by the two pivotal parameters: "parallel separation" and "vertical clearance."

**Part 1:**

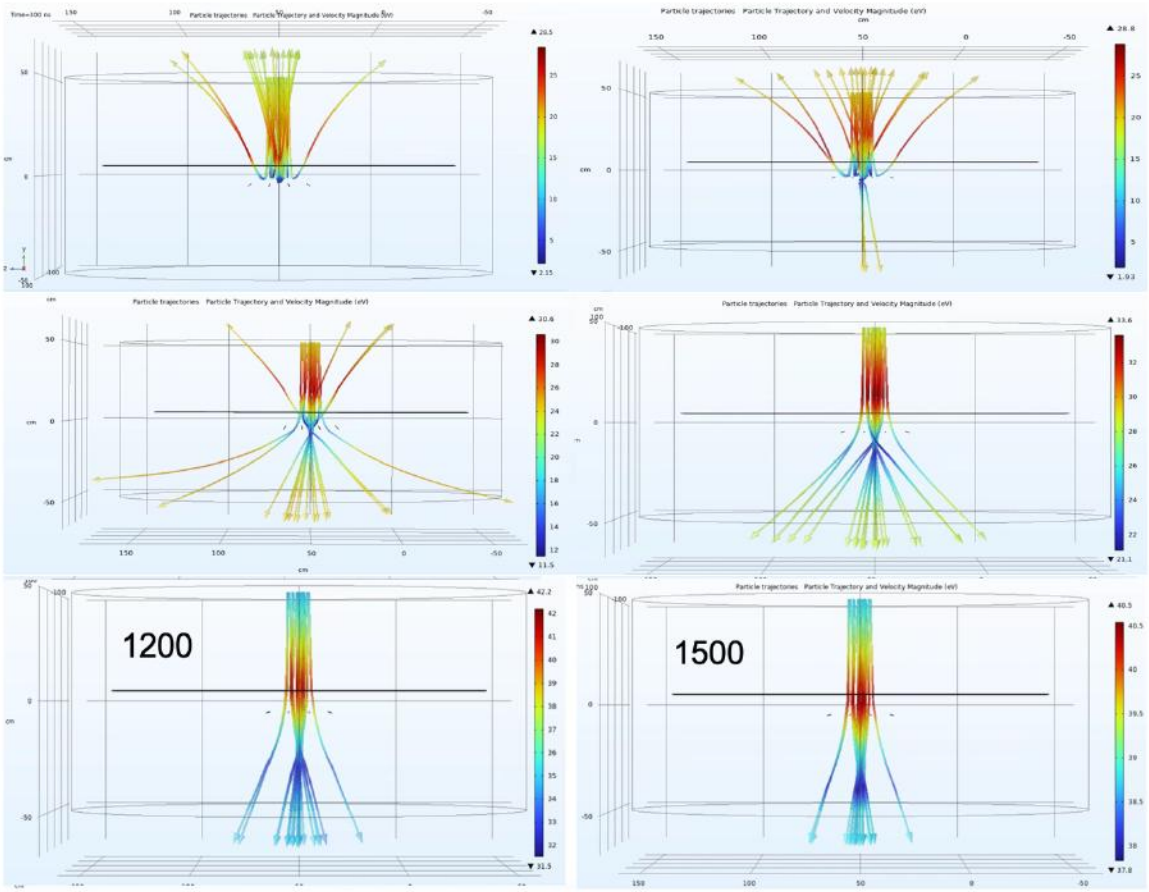

Figure 16 Electron Beams (L to R, EKs of 300eV, 420eV, 600eV, 800eV, 1200eV, 1500eV)

In this part, the critical energy threshold for achieving "complete blockage" is discerned to be approximately 420 eV. This revelation substantiates the filter's capability to effectively arrest and divert electrons characterized by low kinetic energies. Notably, this determined threshold of 420 eV significantly surpasses the average kinetic energy exhibited by SSEs (~10 eV). Furthermore, an additional discovery is made: the threshold energy required for "complete passage" or "escape" registers at around 800 eV. It is pertinent to highlight that this filter operates akin to an optical lens for charged particles.

Specifically, while all electrons can successfully traverse the initial layer (positively charged, thereby attracted to electrons), their trajectory is subsequently influenced as they encounter the second layer (negatively charged, leading to repulsion from electrons). However, due to inherent limitations in the initial model settings, the computation of the transmission probability (i.e., the ratio of the number of escaped particles to the total number of released particles) could not be carried out automatically.

Here's the detailed electron beam parameters:

- Number: 20 per release
- Distribution: KV, Twiss (1m, 1mm)
- Location: -y direction, 50cm above central xy-plane
- Time Range: (0, 20, 300) ns

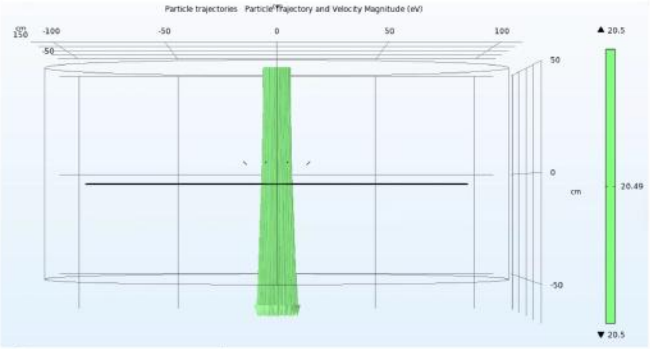

Figure 17 Raw Electron Beam

For comparison and verification, Figure 17 shows the original beam shape of a 420eV electron beam with zero electric field present. Every wire is set to a potential of 0V so that no electrostatic field exists.

**Part 2:**

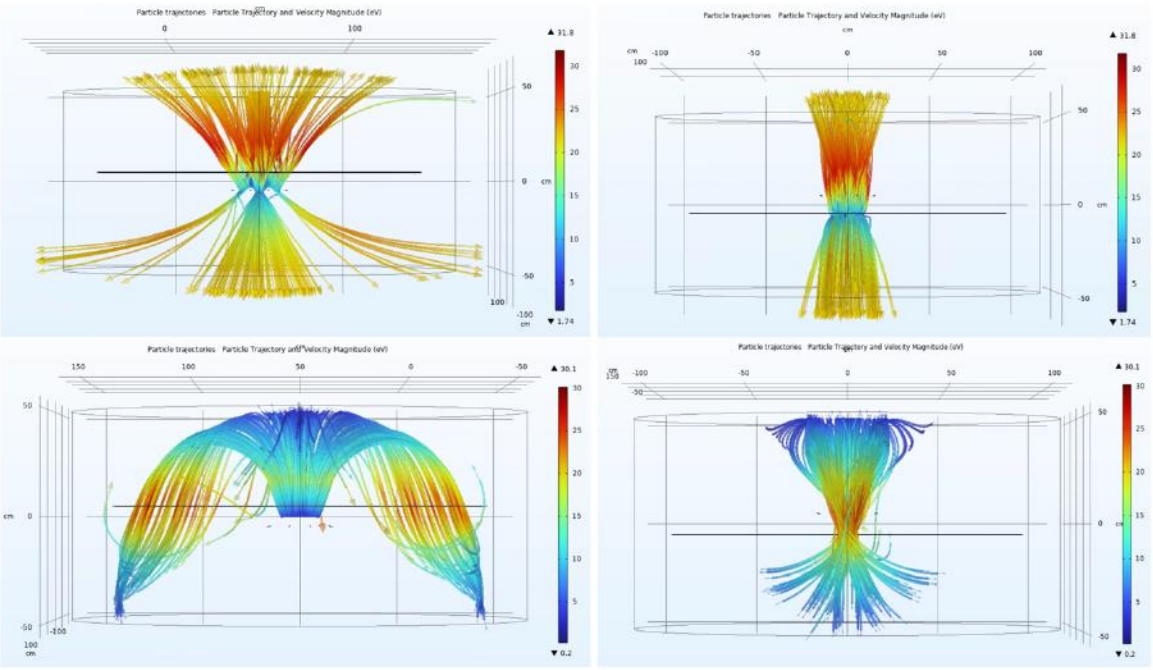

Figure 18 Dense Electron Beam (Upper two @500eV, lower two @10eV)

In this section, a substantial augmentation in the number of released electrons, from 20 to 500, was executed. This alteration was undertaken to provide a clearer depiction of electron trajectories within the xz and yz planes. The analysis of these trajectories unveils two prominent characteristics.

First, owing to the inherent symmetry of our geometry, the entirety of the spatial distribution adheres to a symmetric pattern.

Second, while our primary focus centers on the central region, it becomes evident that the segments of wire extending beyond this central area exert an influence on electron trajectories. Specifically, these extended portions tend to redirect electrons along the axis of the attracting wires — namely, the upper four positively charged wires. This phenomenon holds particular significance in a more close-to-reality 10eV scenario, where electrons exhibit a propensity to encircle the wires located in the peripheral zones. Notably, this phenomenon runs contrary to the "stop and block" purpose of our filter concept, and its occurrence must be preempted in subsequent design iterations.

**Part 3:**

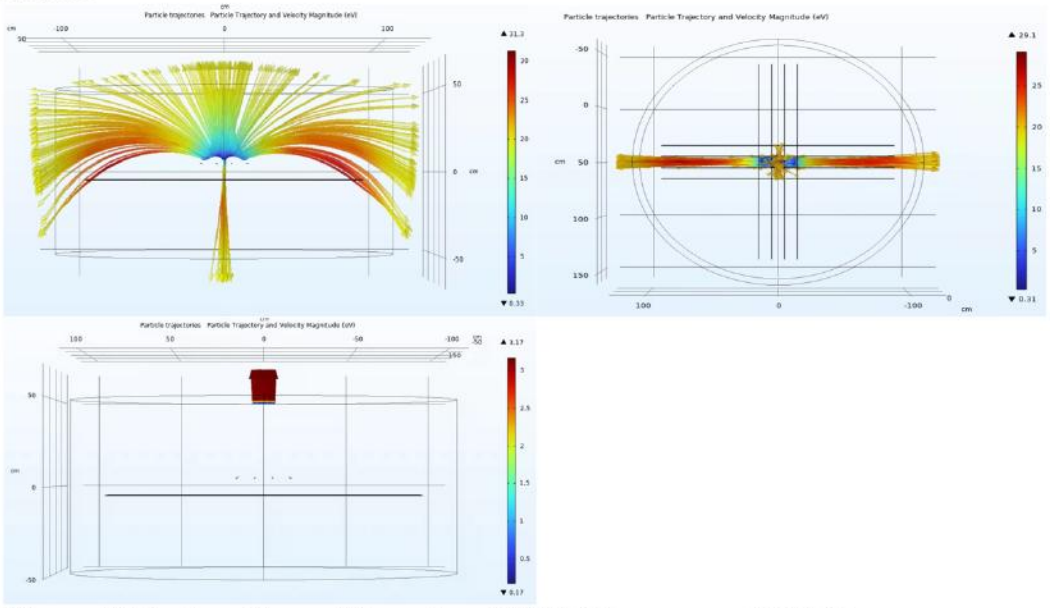

Figure 19 Positron Beam (Upper two @420eV, lower one @10eV)

The use of positrons in the section demonstrates the filter's ability to block particles with either charge, the most important step proving the feasibility of this concept. Analogous to the observations made in Part 2, the determined threshold energy for achieving "complete blockage" hovers around 420 eV. Moreover, a similar particle trajectory along the axis of attracting wires (as in Part 3) — in this instance, the lower four wires — manifests once more. Moreover, in the real-world energy levels such as 10 eV, no particle can even approach the filter.

**Part 4:**

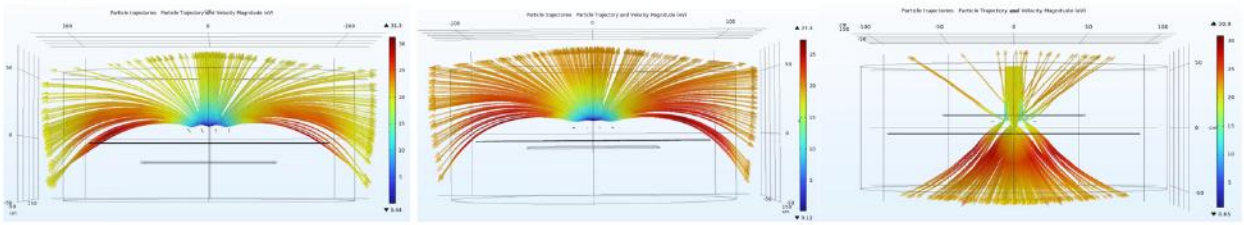

Figure 20 Particle Tracing Trajectories (beam target plane z-coordinate: -20cm, -10cm, +10cm)

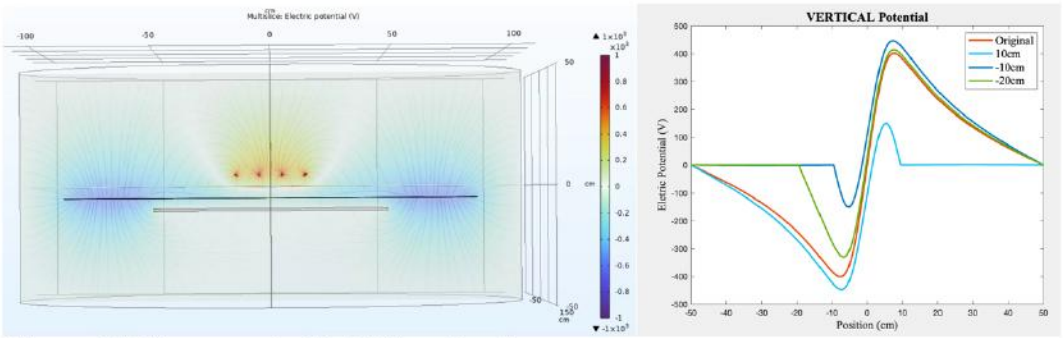

Figure 21 Electrostatic Field Visualization

Utilizing an identical geometry as explored in Parts 1-3, a large grounded square plate is introduced to elucidate the electrostatic field dynamics and particle trajectories within a realistic vacuum chamber setting. This plate is strategically positioned at z-coordinates of -20 cm, -10 cm, and +10 cm, with corresponding potential measurements undertaken.
The introduction of the grounded plate instantaneously creates a rapid decline in the electric potential between itself and the nearest grounded surface, i.e., the vacuum chamber. This reduction brings the field's magnitude close to zero and notably diminishes the maximum potential “on its side.” Furthermore, the presence of the plate contributes to the compression of the field, resulting in a slight elevation of the maximum potential “on the other side."
It is imperative to emphasize that in our prior experiments, the term "maximum potential" encompassed positive and negative values that were equal in magnitude yet bore opposite signs. However, the addition of the grounded plate disrupts this symmetry, rendering the two values no longer equivalent.

Most importantly, this effect raises the demand for voltage on the wire layers close to the beam target. For instance, in the case where the plate is positioned at -10 cm, preserving the condition of "complete blockage" for charged species below 420 eV necessitates an elevation in the potential of negatively charged wires. Meanwhile, the positively charged wires could continue to maintain a potential of 1000 V. It's worth noting that researchers may opt to streamline their analysis by substituting the originally tested "maximum potential" (400 V), as outlined and summarized in Table 1, with the "least maximum potential" (~130 V for the -20 cm case).

**Part 5:**

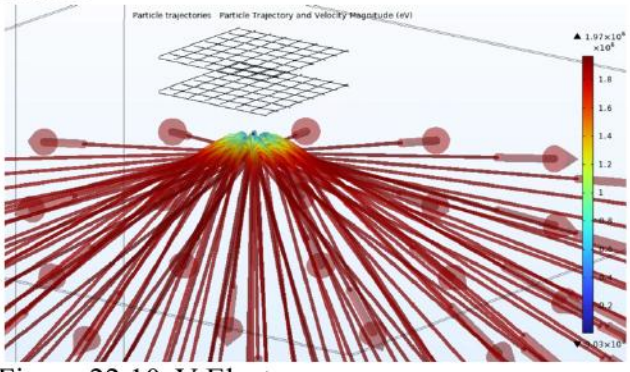
Figure 22 10eV Electrons

Since SSEs in the reality are often emitted in random directions from the beam target plane, a hemispherical release mechanism is adopted to replace the mono-directional incident beams. The effect described in Part 2 is eliminated by cropping the peripheral wires and switching to a more powerful geometry as in Figure 14 (Table 1, Set 5, 58% max potential, the unit has been switched from cm to inch with numbers constant, ps=1in, vc=2in). Note that the supplied voltage has changed from 1000V to 50V.

Figure 22 describes the release of three hundred 10eV electrons from the beam target surface. All particles are effectively obstructed, with minimal distance traversed towards the lower grid. This outcome underscores how the incorporation of a greater number of wires and a sturdier geometric configuration furnishes a more robust shielding against SSEs. Drawing from the insights gained in earlier segments, it stands to reason that had positrons been utilized, the blockage would persist.

However, one last simulation needs to be done in dealing with particles characterized by varying mass and charge. Given that most SSE particles carry a charge of ±1, it becomes imperative to launch several heavier particles for testing. Further details regarding the specific species under examination can be referenced in Figure 2.

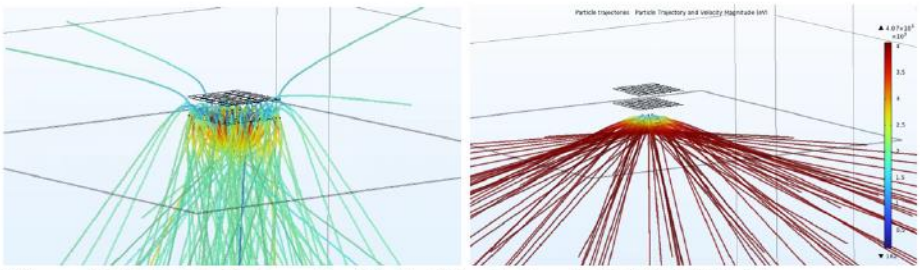
Figure 23 EMI+ Cation (Left) & IM- Anion (Right) @10eV

In Figure 23, three hundred EMI+ Cation (120amu) and IM- Anion (240amu) are tested at 10eV respectively. Almost all launched species are successfully blocked. Even in the case of the four liberated cations, although they manage to evade from the edges, they are markedly diverted towards the xy-plane. This resounding outcome serves as a substantial confirmation of the viability and effectiveness of the proposed biased filter concept.

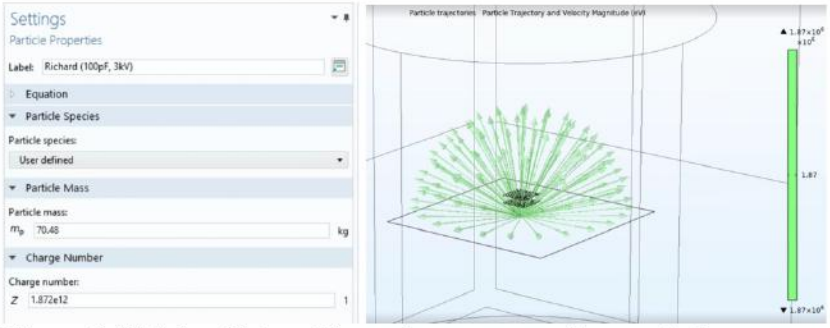

Figure 24 Richard himself as a human capacitor particle

Lastly, one may question if how exactly the particles are being “hemispherically released.” As the purpose of Figure 17, the unaffected trajectory of the hemispherically released particles is

shown in Figure 23, where the particle being released is me (I googled the average capacitance of a human body lol).

One more thing before manufacturing the filter is to clearly see how parallel separation and vertical clearance are affecting our maximum potential. A parameter sweep is performed by modifying the geometry in Part 5, and a phase diagram is made as in Figure 25. Researchers will be able to choose their parameters to optimize performance in different laboratory scenarios.

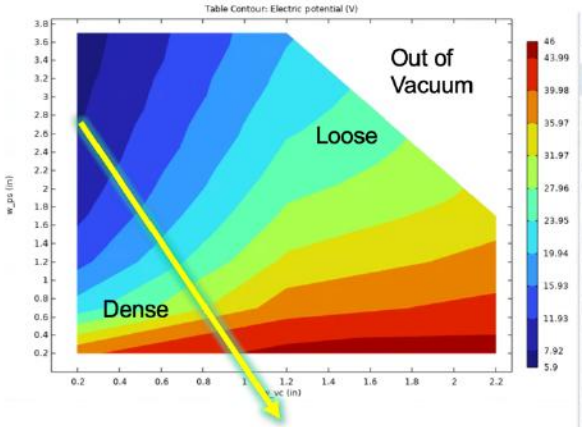


Figure 25 Phase Diagram

Label: Domain Geometry

**YES = SIGNIFICANT**
**NO = No Effect**
**Min = Yes, but Minimal**
**X = Yes, but Irrelevant**

Parameters

| Name | Expression | Value | | Description |
|---|---|---|---|---|
| w_pl | 8 | 8 | Min | Wires Per Layer |
| w_l | (w_pl-1)*w_ps | 0.1778 m | X | Wire Length |
| w_d | 0.005[in] | 1.27E-4 m | NO | Wire Diameter |
| w_r | w_d/2 | 6.35E-5 m | NO | Wire Radius |
| w_vc | 1[in] | 0.0254 m | YES | HALF Vertical Clearance |
| w_ps | 1[in] Side Length | 0.0254 m | YES | Parallel Separation |
| v_r | 50[in] | 1.27 m | NO | Vacuum Radius |
| v_h | 100[in] | 2.54 m | NO | Vacuum Height |
| w_ly | 2 | 2 | X | Number of Layers |
| y_gp | -w_vc-w_gp | -0.127 m | X | Ycoord BT |
| w_gp | 4[in] | 0.1016 m | X | Dis BT to Bottom Grid |

Figure 26 Summary of Parameters' Weight

**Stage Epsilon (Solidworks Manufacturing)**

While the manufacturing aspect is relatively straightforward and not the primary focus of this report, a concise overview of the Solidworks model has been compiled in accordance with the stipulated requirements. The representation entails three rectangular boxes, sequentially denoting the design components of the beam target. These components, presented from top to bottom, encompass the following: normal carbon foam, dense carbon foam featuring minute pores, and a thin aluminum backplate. Significantly, the biased filter is constructed directly atop this assembly and secured in place through the utilization of ceramic insulating stands.

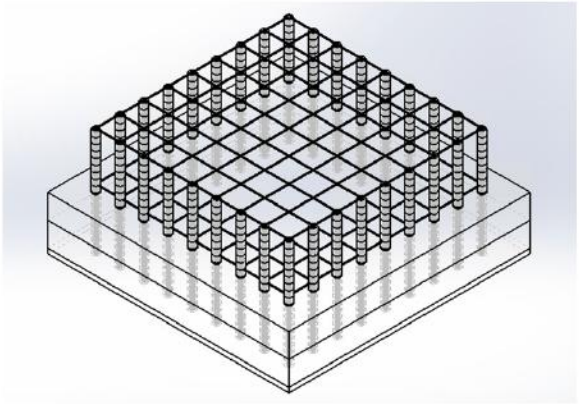

Figure 27 Solidworks Model

## Conclusions

The viability of the biased filter concept for mitigating Secondary Species Emission (SSE) has been substantiated through a combination of theoretical analysis and comprehensive COMSOL simulations. The investigative process has yielded numerous valuable insights and lessons. The most important findings, delineating the essential guidelines for designing the filter geometry, are succinctly compiled within Table 1, along with the conclusive phase diagram (Figure 25). It is the author's sincere wish that this concept could be assisting a multitude of researchers in rectifying inaccuracies induced by SSE across a diverse array of laboratory contexts.

## Acknowledgements

The author, Richard Zhu Ziyi (Northwestern '26), expresses profound gratitude for the invaluable guidance, insights, and trust extended by Adam Collins, Richard Wirz, and fellow researchers at the Plasma and Space Propulsion Laboratory (UCLA PSPL), University of California, Los Angeles. Additionally, heartfelt appreciation is extended to the author's family for unwavering support, both as a researcher and as an individual, throughout his freshman year. Given that this marks my inaugural endeavor in composing a formal research report in English, I kindly beseech your pardon for any inadvertent linguistic nuances.

## Important Mental Lessons

1. If you are confused, do the thing, instead of just thinking randomly and not progressing.

2. Don’t go too theoretical in an engineering problem.

3. Don’t procrastinate (you are spending too much time thinking and worrying this year!)

## Future Expectations

1. There could be potentially more efficient geometries.

2. Find out if there would be a way to establish a quantitative theory regarding the potential distribution.

3. Get this concept patent submitted, reviewed, and published.

4. Build and test it if situation permits (back at UCLA on late September or at Northwestern).

## References

[1] N. M. Uchizono, P. L. Wright, A. L. Collins, R. E. Wirz; Emission spectra of glows produced by ionic liquid ion sources. Appl. Phys. Lett. 10 October 2022; 121 (15): 154101. https://doi.org/10.1063/5.0096595

[2] N. M. Uchizono, A. L. Collins, C. Marrese-Reading, S. M. Arestie, J. K. Ziemer, R. E. Wirz; The role of secondary species emission in vacuum facility effects for electrospray

thrusters. *Journal of Applied Physics* 14 October 2021; 130 (14): 143301. https://doi.org/10.1063/5.0063476

[3] COMSOL official documents